ELSEVIER

Ceramics International 27 (2001) 577–584

CERAMICS INTERNATIONAL

www.elsevier.com/locate/ceramint

Fabrication of graded porous ceramics using alumina–carbon powder mixtures

K. Maca [a], P. Dobsak [a], A.R. Boccaccini [b,*]

[a] *Department of Ceramics, Brno University of Technology, Technicka 2, 616 69 Brno, Czech Republic*
[b] *Department of Materials, Imperial College of Science, Technology and Medicine, London SW7 2BP, UK*

Received 18 September 2000; received in revised form 12 October 2000; accepted 4 December 2000

Abstract

Green bodies consisting of mixtures of submicrometric alumina powder and carbon coal were prepared by cold isostatic pressing. Sintering in air atmosphere resulted in alumina ceramics with controlled porous structure and a highly homogenous distribution of pores. Sintering in vacuum (at 1 to 5 Pa) followed by sintering in air for 2 h at 1530°C led to a graded porous structure. These samples exhibited a highly porous core and a dense surface layer. The conditions of thermodynamic equilibrium for the chemical reactions occurring in the studied system during sintering were calculated. These were used to explain the formation of the graded porosity.

Keywords: A. Sintering; B. Porosity; D. Al_2O_3

1. Introduction

In addition to open-pore containing ceramic materials which are mainly used as filters, membranes, sensors and in thermal protection systems [1,2], there are several other application areas where ceramics and glasses containing closed, isolated pores are needed. For example, one approach proposed to decrease the dielectric constant of glasses and glass-ceramics used as substrates in electronic packaging is the incorporation of porosity [3]. For this application, the pores must be isolated to prevent environmental attack (hermeticity) and to allow for internal wiring network [3]. Materials containing closed porosity of controlled size and well-defined shape are also important for the purpose of calibration and sensitivity assessment of microstructure inspection instruments and techniques, including optical microscopy and X-ray refraction analysis [4].

In other application areas, porous ceramics and glasses are attractive materials when high thermal shock resistance [5–7] or high thermal insulation [1] is required, including applications as thermal barrier coatings [8]. In addition, porous biomaterials (e.g. porous hydroxyapatite) with controlled amount of both closed and open porosity are needed for some implant applications [9–11]. Here, closed porosity helps to match the elastic constants of the implant to that of the bone [10].

A special type of porous ceramics is that of materials exhibiting graded or layered porous structures. These are a special case of functionally graded materials and they are interesting for several applications. They can be used, for example, for cores for precision casting of highly reactive alloys, where the dense surface protects the component against metal penetration and the porous centre facilitates leaching out the ceramic after solidification of the metal improving also the crushability characteristics of the core [12,13]. Applications of graded porous ceramics for especial heat insulation structures [14], high thermal shock resistant components [15,16] and thick thermal barrier coatings [8] have been also proposed. Ceramics with graded porous structures are also considered for controlled variation of optical transmission properties in luminiscent thin films [17], as well as for biocompatible porous implants [18]. Graded porous ceramics can also serve as the starting preforms for the fabrication of functionally graded materials, which are produced by liquid metal infiltration of suitable porous preforms [19,20].

* Corresponding author. Tel.: +44-020-7594-6731; fax: +44-020-7584-3194.
E-mail address: a.boccaccini@ic.ac.uk (A.R. Boccaccini).

0272-8842/01/$20.00
PII: S0272-8842(01)00004-9

The variety of application options for ceramics containing pores, including graded porous ceramics, as described above, has originated numerous processing strategies for their fabrication during the last years. These have been extensively reviewed by Rice [21], Saggio-Woyansky et al. [1] and by Sepulveda [2]. In particular, graded porous ceramics are usually created by packing ceramic powders or fibres to varying densities followed by partial sintering [19,20,22]. More sophisticated techniques have been also proposed, including: multilayer lamination of individual tapes [20,23], use of thin sheets containing percolating pyrolyzable particles [20], sintering of laminated green tapes with layer by layer modification of the sintering behaviour by addition of different amount of additives [17] and electrochemical processing [18].

In the present work, porous alumina ceramics are obtained by controlled sintering of alumina–carbon powder mixtures. Besides the traditional method of developing porosity by burning out carbon fugitive inclusions during sintering in air, it is shown that heat-treatment of the mixtures in low-oxygen atmosphere leads to alumina ceramics with a graded porous structure. The mechanism of formation of the graded porous structure, based on thermodynamic considerations, is explained in detail.

2. Experimental

Powder mixtures were prepared using alumina powder ($d_{50}=0.6$ μm, type RC HPDBM, Malakoff Industries, USA) and milled carbon coal ($d_{50}=2.8$ μm, type GA-1) or as-received carbon coal ($d_{50}=13$ μm, type Kolorex K), both from SLZ, Slovak Rep. The mixtures were milled with alumina balls for a period of 30 h. Subsequently, organic binder (Stearin, Merck, Germany) was added and milling continued for another 10 h. The composition of the mixtures and their designation are given in Table 1.

Experimental bodies in the shape of cylinders (diameter: 40 mm, height; 10–15 mm) were formed by cold isostatic pressing (250 MPa/30 s) and then grounded to the shape of prisms. The relative green density of the specimens was obtained by two methods; (i) dividing the weight of the alumina–carbon mixture by the volume of the body and then dividing it by the theoretical density of the alumina–carbon mixture ($\rho_{rel}-1$); and (ii) dividing the weight of alumina by the volume of the sample and then by the theoretical density of alumina ($\rho_{rel}-2$).

Some of the bodies were presintered in air atmosphere at a temperature of 800°C for a period of 1 h followed by sintering in air at a temperature of 1530°C for a period of 2 h. The heating rate was 5°C/min up to 1450°C, then 2°C/min up to the final temperature. The final sintered density was calculated by means of measuring the dimensions and weight and also by the water immersion technique. The Young's modulus of selected porous samples was measured using a universal testing equipment (Z 020, Zwick, Germany) in three-point bending, according to the norm EN 843-2. The span of supports was 20 mm. The samples had prismatic shape with cross-sections of 2×3 mm^2 and 3×4 mm^2.

A second group of samples was not presintered in air but directly heated in a vacuum furnace at pressures of 1 to 5 Pa. The same heating schedule as before was used. The only difference was the soaking time at 1530°C, which was of 4 h. After vacuum sintering, the samples were submitted to an additional heat treatment in air atmosphere at 1530°C during 2 h. The weight loss was measured after both heating steps. The linear shrinkage was evaluated by measuring axial dimensions. The microstructure of sintered samples was studied by means of scanning electron microscopy (SEM) (Philips XL30, The Netherlands) on grounded cross-sections.

Table 1
The composition of used powder mixtures

Mixture	Alumina		Carbon coal		Stearin
	wt.%	vol.%	wt.%	vol.%	wt.%
A90C10	89.5	88.2	10.5	11.8	2.5
A90C10 (as-rec)	89.5	88.2	10.5	11.8	2.5
A70C30	70.0	67.3	30.0	32.7	2.5

3. Results

3.1. Properties of green bodies

The relative densities of the samples after cold isostatic pressing are given in Table 2. The values in Table 2 indicate that the particle size of carbon did not influence the packing density of the pressed compacts. The lowest packing density by both methods was determined for the sample with the highest content of carbon.

3.2. Properties of sintered bodies

The values of relative final densities and axial shrinkage of samples sintered in air are given in Table 3. The values in Table 3 show that the relative densities determined by the water immersion method were always

Table 2
Relative densities of green bodies referred to the theoretical density either of the alumina–carbon mixture ($\rho_{rel}-1$) or of pure alumina ($\rho_{rel}-2$) after cold isostatic pressing

Mixture	$\rho_{rel}-1$ (%)	$\rho_{rel}-2$ (%)
A90C10	46.3	42.0
A90C10 (as-rec)	45.6	41.0
A70C30	35.7	25.7

Table 3
Relative sintered densities and axial shrinkage of samples sintered in air

Mixture	$\rho_{rel}-2$ (%) (by measuring dimensions)	$\rho_{rel}-2$ (%) (by water immersion)	ϵ (%) (axial shrinkage)
A90C10	73.6	81.4	−17.3
A90C10 (as-recieved)	67.8	73.6	−15.0
A70C30	61.1	62.6	−24.7

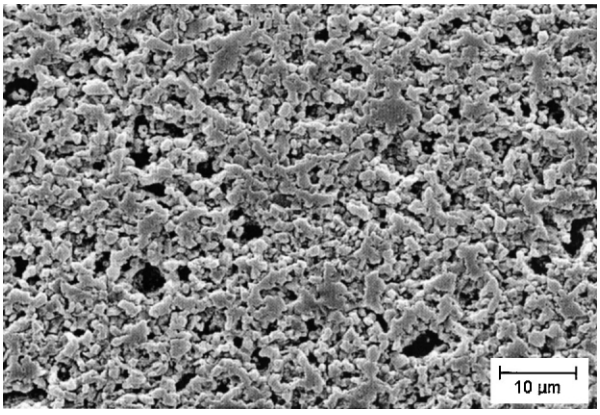

Fig. 1. Microstructure of the cross-section of the A90C10 sample (89.5 wt.% Al_2O_3 + 10.5 wt.% C) after sintering in air at 1530°C/2 h.

higher than those ascertained by measuring the weight and dimensions of the samples. The highest final density was exhibited by the sample containing 10.5 wt.% of milled carbon coal. The Young's modulus of this sample was 150 GPa.

Typical microstructures of the porous ceramics after sintering in air are shown in Figs. 1–3. If milled carbon coal was used, the distribution of pores was homogenous irrespective of carbon content (Figs. 1 and 2). The mean size of pores was less than 5 μm in both cases. The grain size of the alumina matrix was about 2 μm in the case of 10.5 wt.% carbon content (Fig. 1) and about 1 μm in the case of 30 wt.% carbon content (Fig. 2). The microstructure of samples with 10.5wt% of as-received carbon coal was highly non-homogenous (Fig. 3). Pores with diameters in the range 20–40 μm were found in this sample. However, the ceramic grain size was very fine (≅ 1 μm).

The samples sintered in vacuum showed a different densification behaviour and different porosity structure. The density measured for the sample A90C10 after sintering in vacuum was 2.0 g cm^{-3}. For comparison, the density of the samples sintered in air was 2.9 g cm^{-3} ($\rho_{rel}-2 = 73.6\%$, see Table 3). The linear shrinkage during sintering in vacuum was −7.5%. The mass losses during sintering in vacuum and subsequent heat-treatment in air for the sample A90C10 are given in Table 4. The value of $\Delta m_1 = 16.1\%$ after vacuum sintering consists of a mass loss of 2.5% of organic binder while the

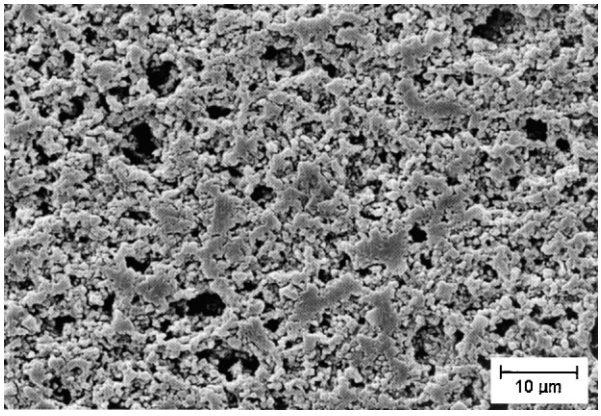

Fig. 2. Microstructure of the cross-section of the A70C30 sample (70 wt.% Al_2O_3 + 30 wt.% C) after sintering in air at 1530°C/2 h.

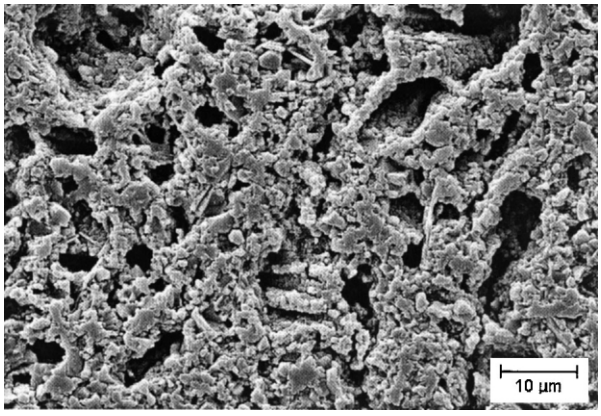

Fig. 3. Microstructure of the cross-section of the A90C10 (as-received) sample (89.5 wt.% Al_2O_3 + 10.5 wt.% of as-received coal) after sintering in air at 1530°C/2 h.

rest (13.6%) is attributed to the mass losses of carbon and alumina, as discussed in the next section.

Typical microstructures of the ceramics sintered in vacuum followed by heat-treatment in air are shown in Fig. 4(a)–(e). The material exhibits a graded porous structure, as seen in Fig. (4a) and (b). The formation of a relatively dense surface layer of 15–20 μm thickness with grain sizes in the range 2.5–5 μm is documented in Fig. 4(b) and (c). The grain size is seen to decrease towards the centre of sample. The grain size in the sample centre is ≅ 2 μm [Fig. 4(e)], while at a distance of about 0.6 mm from the sample centre, the grains are 2 to 3 times larger [Fig. 4(d)].

4. Discussion

4.1. Sintering in air atmosphere

The use of organic inclusions such as PVC granules as fugitive fillers is a traditional technique employed to fabricate porous ceramics [3,4,9,24]. The direct use of carbon particles (or fibres) to create "artificial porosity",

Table 4
Mass loss during sintering in vacuum and subsequent heat treatment in air

Mixture	After pressing	After sintering in vacuum		After subsequent heat-treatment in air	
	m_0(g)	m_1 (g)	Δm_1 (%)	m_2 (g)	Δm_2 (%)
A90C10	8.136	6.858	16.1	6.660	2.5

on the contrary, has been less investigated [21,25]. The porosity of carbon containing samples sintered in air arises mainly due to the reaction of carbon with the oxygen in air atmosphere, according to the reaction:

$$2\underset{\text{solid}}{\langle C\rangle} + \underset{\text{gas}}{\{O_2\}} \leftrightarrow 2\underset{\text{gas}}{\{CO\}}\ . \tag{1}$$

In these samples, both open and close porosity develop, as the higher values of relative densities obtained by water immersion method, in comparison with measuring of weight and dimensions, reveal (Table 3). It can be assumed that the sintering of alumina, which occurs by a mechanism of diffusion, takes place simultaneously with the burning out of carbon. Assuming that the shrinkage of the body is isotropic during sintering (and in the case of cold isostatic pressing and isotropic shape of particles there is no reason a priori for anisotropy effects), the final relative density [ρ_f (%TD)] can be calculated from the green relative density [ρ_0 (%TD)] and the axial shrinkage [ε (%)] by means of the following equation:

$$\rho_f = \rho_0 \cdot \left(\frac{100}{100+\varepsilon}\right)^3 \tag{2}$$

Table 5 shows the comparison of measured final densities with those calculated according to Eq. (2). The differences between measured and calculated final relative densities, as shown in Table 5, are given mainly by the experimental errors in determining the densities and shrinkage data. From this comparison, it is confirmed that shrinkage during sintering was isotropic.

The samples fabricated by using milled carbon inclusions exhibited equiaxed and homogeneously distributed porosity (Figs. 1 and 2). The Young's modulus of porous materials is affected by the volume fraction and shape of the pores [21,26]. Assuming that the pores are spherical, and taking the published value $E = 360$ GPa for dense samples (>99%TD) prepared from the same alumina powder [27], a model reported in the literature [26] predicts a Young's modulus $E(P) = 175$ GPa for a porous sample with 26.4% porosity. This value is about 15% higher than the measured value (150 GPa), indicating that the pores deviate from the assumed perfect spherical shape, as observed in the micrographs (e.g. in Fig. 1). A further assessment of pore shape would require quantitative microstructural analysis and stereological calculations, but this was not conducted here.

Table 5
The measured and calculated final relative densities of porous ceramics

Mixture	ρ_f (%TD) measured	ρ_f (%TD) calculated
A90C10	73.6	74.3
A90C10 (as-rec)	67.8	67.3
A70C30	61.1	60.2

The results confirm, nevertheless, that sintering alumina–carbon powder mixtures in air is a suitable method for obtaining porous ceramics with controlled and homogeneously distributed porosity. It must also be pointed out that the size distribution of the pores reflects in some extension the size distribution of carbon particles, as expected. This part of the study demonstrates also that fine (milled) carbon particles should be used to warrant adequate control of the pore size, shape and distribution.

4.2. Sintering in vacuum

Vacuum sintering of a mixture of 89.5 wt.% Al_2O_3 and 10.5 wt.% carbon at 1 to 5 Pa and subsequent heat-treatment in air led to a graded porous structure. The samples exhibited a highly porous core and a dense surface layer [Fig. 4(a) and (b)]. This result is significant because it indicates that the present processing approach represents a convenient and simple way to fabricate in-situ porous graded ceramics. As mentioned in the introduction, graded porous ceramics are usually obtained by packing ceramic powders and/or fibres to varying densities followed by partial sintering [19,20,22]. The main disadvantage of this layer-structure approach, however, is the differential shrinkage occurring between layers with different porosity levels, which causes warping and cracking of the preforms [20]. More complex techniques have been tried recently to fabricate ceramics with layered or graded porosity. These include, for example, multilayer lamination of individual tapes [18,20], sintering of laminated green tapes with layer by layer modification of the sintering behaviour by addition of different amount of additives [17] and electrochemical processing of conducting and nonconducting substrates [23]. Tailored porosity gradients have been also obtained by colloidal infiltration of molded polymer sponges, followed by pyrolysis of the sponge and sintering of the ceramic [28]. An other technique developed for obtaining anisotropic porous structures is based on liquid Si infiltration of porous carbonised wood templates [14].

The development of the graded porous microstructure in our materials relies on the use of a low partial pressure of oxygen during sintering, as discussed next.

With decreasing partial pressure of oxygen and increasing temperature, carbon will tend to react with

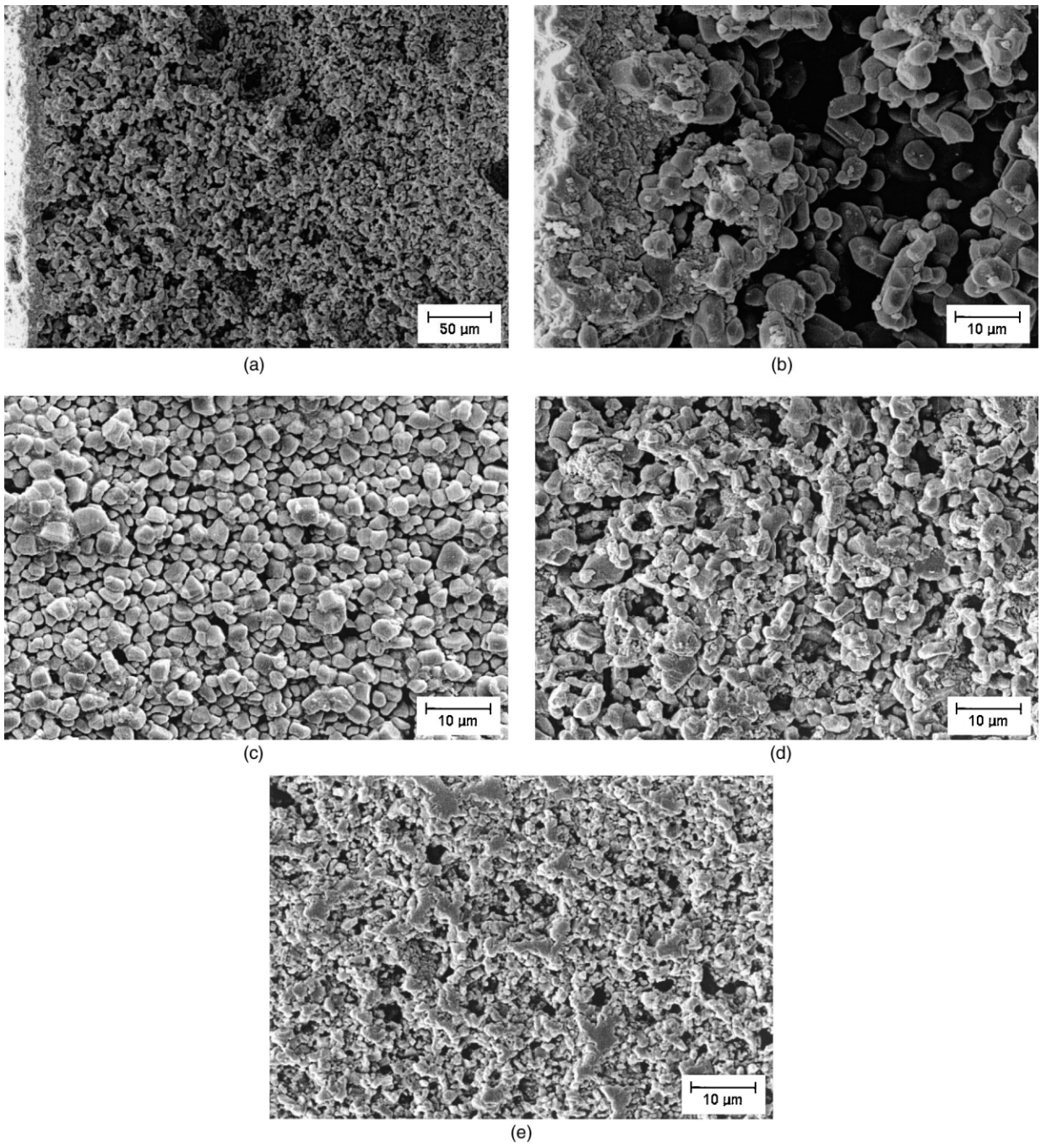

Fig. 4. SEM micrographs of different microstructures of the A90C10 sample (89.5 wt.% Al_2O_3 + 10.5 wt.% C), after sintering in vacuum (1530°C/4 h) followed by heat-treatment in air (1530°C/2 h), showing: (a) formation of a graded porous structure, (b) porous area at a distance of 0–75 μm underneath the sample surface, (c) region of high densification, (d) porous area at a distance of about 600–675 μm underneath the sample surface, (e) porous area at the centre of the sample.

alumina rather than with oxygen [see Eq. (1)], according to the following reaction:

$$\underset{\text{solid}}{\langle Al_2O_3\rangle} + 2\underset{\text{solid}}{\langle C\rangle} \leftrightarrow \underset{\text{gas}}{\{Al_2O\}} + 2\underset{\text{gas}}{\{CO\}} \quad (3)$$

The formation of Al_2O is more probable than formation of other existing gaseous products (such as AlO, Al_2O_2), according to thermodynamic calculations using the Barin's data of Gibbs free energies of pure substances [29]. In order to decide which of the two possible reactions [Eq. (1) or (3)] is more probable (and will dominantly occur), it is advisable to subtract both reactions. The result is given by:

$$\underset{\text{gas}}{\{Al_2O\}} + \underset{\text{gas}}{\{O_2\}} \leftrightarrow \underset{\text{solid}}{\langle Al_2O_3\rangle} \quad (4)$$

The thermodynamic equilibrium of Eq. (4) can be calculated by the Van't Hoff isotherm [30]:

$$\Delta G = \Delta G^0 + RT\ln\frac{a_{Al_2O_3}}{a_{Al_2O}\cdot a_{O_2}} \quad (5)$$

where R is the universal gas constant (8.314 J K^{-1} mol^{-1}), a are activities and ΔG^0 (kJ) is the reaction change of standard Gibbs free energy of substances in pure state (for gases it means the pressure of 1 atm).

The Al_2O_3 component is in its pure state, so its activity is equal to 1, while the activities of gases are given by their partial pressures:

$$a_{Al_2O} = p_{Al_2O}(\text{atm}), \quad a_{O2} = p_{O2}(\text{atm}). \quad (6)$$

In equilibrium, $\Delta G = 0$, thus from Eqs. (5) and (6)] it is possible to write:

$$\frac{1}{p_{Al_2O}\cdot p_{O_2}} = e^{\frac{-\Delta G^0}{RT}}. \quad (7)$$

From stoichiometry of the reaction given by Eq. (4), the partial pressures of Al_2O and O_2 are equal and the following results:

$$p_{O_2}(\text{atm}) = p_{Al_2O}(\text{atm}) = e^{\frac{\Delta G^0}{2RT}} \quad (8)$$

ΔG^0 can be calculated with the help of Barin's data [29]. After regression, it can be given by the following expression:

$$\Delta G^0(\text{J}) = -1515000 + 377 \quad \text{T(K)} \quad (9)$$

The dependence of the equilibrium oxygen partial pressure on the temperature for the reaction given by Eq. (3) was calculated using Eqs. (8) and (9) and it is shown in Fig. 5. If the conditions in the furnace are situated in the area above the curve of equilibrium of oxygen partial pressure, carbon will react more likely with atmospheric oxygen [Eq. (1)] rather than with alumina [Eq. (3)], and vice versa.

At a temperature of 1530°C, the equilibrium partial pressure of oxygen is obtained:

$$p_{O_2} \cong 7\times10^{-13}\text{atm} \cong 7\times10^{-8}\text{Pa} \quad (10)$$

From the results of weight losses presented in Table 4, it is seen that part of Al_2O_3 was lost during sintering in vacuum. This shows that the reaction given by Eq. (3) effectively occurred during sintering although the partial pressure of oxygen in the furnace was higher than 7×10^{-8} Pa. This should have the following reasons: (i) the partial pressure of oxygen in the centre of the sample is lower than in the furnace atmosphere; and (ii) the reaction given by Eq. (3) occurs simultaneously with the reaction given by Eq. (1), but in a very limited extent so that the amount of reaction products of Eq. (1) is much higher than those of Eq. (3).

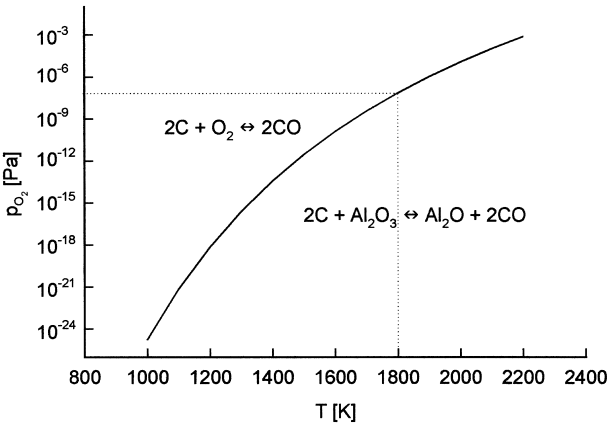

Fig. 5. The dependence of equilibrium oxygen partial pressure on temperature for the reaction $Al_2O + O_2 \leftrightarrow Al_2O_3$.

Both gaseous products of the reaction given by Eq. (3) move towards the sample surface and further towards the vacuum pump. During this migration they can condense at the powder surfaces with high chemical potential by reverse chemical reaction and thus form necks between particles (evaporation–condensation mechanism of sintering). This mechanism increases the strength of the sample but it does not increase sample density.

There is a higher partial pressure of oxygen near the sample surface than inside the ceramic body. Therefore, on the surface the back oxidation of Al_2O [given by Eq. (4)] can occur, which results in the development of the dense surface layer, as clearly seen on the SEM micrographs (Fig. 4a–c). Finally, both the density and mechanical strength of the sample increase during the last sintering step in air. Sintering occurs only by a diffusion mechanism in this step. Thus, based on the experimental results and on the thermodynamic considerations presented above, the optimal processing parameters to fabricate graded porous alumina using the present technique can be controlled.

The results of this study are in agreement with previous work performed on injection molded alumina ceramic cores [12,13], where similar alumina–carbon powder mixtures were used to obtain porous bodies by sintering in hydrogen atmosphere. According to that work [12], the optimal conditions for preparing porous alumina cores with an integral outer barrier layer were as follows: alumina particle size: 1–20 μm, fugitive filler (carbon) particle size: <300 μm, molar ratio of carbon to alumina: 0.2–0.3 (which corresponds to 2.3–4.1 wt.% C), heating rate: 5°C/min, sintering temperatures: 1750–1850°C and soaking time: 2 h. Those authors assumed that at temperatures

higher than 1500°C in hydrogen atmosphere the reaction given by Eq. (3) occurred. It was postulated that the denser layer at the core surface arose due to reaction of Al_2O with oxygen or water vapor present in hydrogen as impurities. It was shown that the thickness of the dense surface layer (between 5 and 100 μm) depended on the starting carbon content, on the firing temperature and time and on the water dewpoint in the furnace atmosphere [12]. The experimental conditions of the present work were different to that of ref. [12] in that smaller alumina and carbon particles were used and vacuum instead of hydrogen was the sintering atmosphere. Indeed, the most significant advantage of the present approach in comparison to that in refs. [12,13] is the use of vacuum instead of hydrogen as sintering atmosphere.

5. Conclusions

Starting with isostatically pressed alumina samples containing different amounts of carbon inclusions, and by means of sintering in air atmosphere, samples with different porosity structures, in terms of size and shape of pores, were fabricated. It was found that 30 wt.% of carbon is excessive for preparing porous alumina samples of sufficient structural integrity. The particle size distribution of carbon particles plays an important role in the final microstructure of the materials: using smaller particles (closer to the size of the alumina particles) leads to more homogenous structures and smaller pores.

The most interesting result of this study is the development of a simple method for preparation of graded porous ceramics. The processing approach includes cold isostatic pressing of mixtures containing 10 wt.% of milled carbon, followed by a sintering stage in vacuum and a final heat treatment in air.

Overall, this study has shown that the key to tailor the microstructure of porous (and graded porous) ceramics prepared from mixtures of carbon and alumina powders is to determine the optimal composition of the mixtures, their homogenisation behaviour, and, most importantly, the sintering conditions.

Acknowledgements

Partial support for this work was provided by the Czech Ministry of Education under Grant No. VZ CEZ: J22/98.

References

[1] J. Saggio-Woyansky, C.E. Scott, W.P. Minnear, Porous ceramics, Ceram. Bull. 71 (11) (1992) 1674–1682.
[2] P. Sepulveda, Gelcasting foams for porous ceramics, Ceram. Bull. 76 (10) (1997) 61–65.
[3] J.K. Yamamoto, K. Kata, Y. Shimada, Fabrication of controlled porosity in a tape cast glass ceramic substrate material, Mater. Lett. 8 (8) (1989) 278–282.
[4] D.J. Roth, E.R. Generazio, G.Y. Baaklini, Quantitative void characterisation in structural ceramics by use of scanning laser acoustic microscopy, Mater. Eval. 45 (8) (1987) 958–966.
[5] A.R. Boccaccini, G. Ondracek, The quantitative microstructure-property correlations of composite and porous materials: an engineering tool for designing new materials, in: R. Pyrz (Ed.), Proc. IUTAM Symposium on Microstructure–Property Interactions in Composite Materials, Aalborg, Denmark, 23–25 August 1994. Kluwer Academic Publishers, 1995, pp. 27–38.
[6] M. Arnold, A.R. Boccaccini, G. Ondracek, Theoretical and experimental considerations on the thermal shock resistance of sintered glasses and ceramics using modeled microstructure-property correlations, J. Mater. Sci. 31 (1996) 463–469.
[7] Y.P. Jin, Y.T. Chou, Thermal and mechanical properties of porous Y-PSZ/zircon composites, Mater. Res. Innovat. 1 (1998) 227–230.
[8] H.-D. Steffens, Z. Babiaka, M. Gramlicha, Some aspects of thick thermal barrier coatings lifetime prolongation, J. Thermal Spray Technol. 8 (1999) 517–522.
[9] D.M. Liu, Control of pore geometry on influencing the mechanical property of porous hydroxyapatite, J. Mater. Sci. Lett. 15 (1996) 419–421.
[10] L. Vaz, A.B. Lopes, M. Almeida, Porosity control of hydroxyapatite implants, J. Mater. Sci. Mater. Med. 10 (1999) 239–242.
[11] N.O. Engin, A.C. Tas, Preparation of porous $Ca_{10}(PO_4)_6(OH)_2$ and β-$Ca_3(PO_4)_2$ bioceramics, J. Am. Ceram. Soc. 83 (2000) 1581–1584.
[12] W.D. Pasco, F.J. Klug, Method for making porous, crushable core having a porous integral outer barrier layer having a density gradient therein, US Patent 4,221,748, 9.9, 1980.
[13] Ch.D. Greskovich, F.J. Klug, W.D. Pasco, Process for making a ceramic article having a dense integral outer barrier layer and a high degree of porosity and crushability characteristics, US Patent 4,187,266, 5.2, 1980.
[14] P. Greil, T. Lifka, A. Kaindl, Biomorphic cellular silicon carbide ceramics from wood: II. Mechanical properties, J. Eur. Ceram. Soc. 18 (1998) 1975–1983.
[15] K. Satyamurthy, D.P.H. Hasselman, Effect of spatially varying porosity on magnitude of thermal stresses during steady state heat flow, J. Am. Ceram. Soc. 62 (1979) 431–432.
[16] A.R. Boccaccini, J. Janczak, D.M.R. Taplin, M. Köpf, The multibarriers-system as a materials science approach for industrial waste disposal and recycling: application of gradient and multilayered microstructures, Environ. Technol. 17 (1996) 1193–1203.
[17] S. Ahne, W. Rossner, P. Greil, Ceramic multilayers with graded porosity and microcavities, in: P. Vincencizini (Ed.), 9th CIMTEC, World Ceramics Congress. Part C, Techna Srl, 1999, pp. 299–304.
[18] J.P. Werner, C. Lathe, P. Greil, Pore-graded hydroxyapatite materials for implantation, Br. Ceram. Proc. 2 (60) (1999) 547–548.
[19] S. Suresh, A. Mortensen, Fundamentals of Functionally Graded Materials, The Institute of Materials, London, 1998.
[20] S.F. Corbin, X. Zhao-jie, H. Henein, P.S. Apte, Functionally graded metal/ceramic composites by tape casting, lamination and infiltration, Mater. Sci. Eng. A262 (1999) 192–203.
[21] R.W. Rice, Porosity of Ceramics, Marcel Dekker, 1998.
[22] D. Muscat, R.A.L. Drew, Modelling the infiltration kinetics of molten aluminium into porous titanium carbide, Metall. Mater. Trans. 25A (1994) 2357–2370.
[23] R. Jedamzik, A. Neubrand, J. Roedel, Production of functionally

graded materials from electrochemically modified carbon performs, J. Am. Ceram. Soc. 83 (2000) 983–985.
[24] R.A. Lopes, A.M. Segadaes, Microstructure, permeability and mechanical behaviour of ceramic foams, Mater. Sci. Eng. A209 (1996) 149–155.
[25] S. Spaseska, M. Milosevski, R. Milosevska, G. Ondracek, in: P. Duran, J.F. Fernandez (Eds.), Third Euro-Ceramics, Vol. 3, Faenza Editrice Iberica, Madrid, 1993, p. 107.
[26] A.R. Boccaccini, Fabrication, microstructural characterisation and mechanical properties of glass compacts containing controlled porosity of spheroidal shape, J. Porous Mater. 6 (1999) 369–379.
[27] J. Cihlar, M. Trunec, V. Sida, Ceramic femoral component of knee prosthesis, in: R.Z. LeGeros, J.P. LeGeros (Eds.), Bioceramics, Vol. 11, World Scientific Publishing Co. Pte. Ltd, New York, 1998, pp. 69–72.
[28] F. Cichocki Jr., K.P. Trumble, J. Roedel, Tailored porosity gradients via colloidal infiltration of compression-molded sponges, J. Am. Ceram. Soc. 81 (1998) 1661–1664.
[29] I. Barin, Thermochemical Data of Pure Substances, VCH Verlagsgessellschaft mbH, 1993.
[30] L. Zemcik, K. Rusin, J. Svejcar, Prediction of the reactivity between melt and refractory material from the viewpoint of physical chemistry, in: Proc. of 56th World Foundry Congress, Verein Deutscher Giesserfachleute, Duesseldorf, 1989, pp. 181–189.